Journal of Dentistry 151 (2024) 105411

Contents lists available at ScienceDirect

Journal of Dentistry

journal homepage: www.elsevier.com/locate/jdent

A 3D *in vitro* model of biphasic calcium phosphate (BCP) scaffold combined with human osteoblasts, osteoclasts, and endothelial cells as a platform to mimic the oral microenvironment for tissue regeneration

Domitilla Mandatori [a,1,*], Emira D'Amico [a,1], Tea Romasco [a], Maria Laura Gatto [b], Maria Pina Notarangelo [c], Carlo Mangano [d], Michele Furlani [e,2], Letizia Penolazzi [c,2]

[a] Department of Medical, Oral and Biotechnological Sciences, Center for Advanced Studies and Technology CAST, "G. d' Annunzio" University Chieti- Pescara, 66100 Chieti, Italy
[b] Department of Science and Engineering of Materials, Environment and Urban Planning, Università Politecnica delle Marche, 60131 Ancona, Italy
[c] Department of Neuroscience and Rehabilitation, University of Ferrara, 44121 Ferrara, Italy
[d] Department of Dental Sciences, University Vita Salute San Raffaele, Milan, Italy
[e] Department of Odontostomatologic and Specialized Clinical Sciences, Università Politecnica delle Marche, 60131 Ancona, Italy

ARTICLE INFO

Keywords:
Biphasic Calcium Phosphate (BCP)
Scaffold
3D printing
Tissue engineering
Jawbone regeneration

ABSTRACT

Objectives: This study aimed to develop an innovative 3D *in vitro* model based on the biphasic calcium phosphate (BCP) scaffold combined with human osteoblasts (hOBs), osteoclasts (hOCs), and endothelial cells to evaluate its effects on bone and vascular cells behavior.
Methods: To this end, an optimized mixture of hydroxyapatite (HA) and β-tricalcium phosphate (TCP) with a weight ratio of 30/70 was employed to develop a BCP scaffold using the computer-aided design (CAD) approach. The BCP scaffold was combined with primary cultures of hOBs, hOCs and human umbilical vein endothelial cells (HUVECs).
Results: Morphometric analyses using scanning electron microscopy (SEM) and X-ray micro-computed tomography, along with biomechanical testing, revealed that BCP scaffold exhibited a regular 3D structure with large interconnected internal pores (700 μm) and high mechanical strength. In terms of biological behavior, after 14 days of tri-culture with hOBs, hMCs and HUVECs, SEM, immunofluorescence, and histological analyses showed that all cell types were viable and adhered well to the entire surface of the scaffold. Interestingly, SEM and energy-dispersive X-ray spectroscopy analyses also revealed on the BCP scaffold the presence of mineralized matrix crystals of Ca, P, O and C within a tissue-like cell layer produced by the interaction of the three cell types.
Conclusions: Data confirmed the high performance of the BCP scaffold through biomechanical studies. Notably, for the first time, this study demonstrated the feasibility of combining BCP scaffold with hOBs, hOCs, and HUVEC, which remained viable and maintained their native phenotypes, creating also tissue-like cell layer.
Clinical significance: Although further investigation is needed, these results underscore the potential to develop a 3D *in vitro* model that mimics the oral microenvironment, which could be valuable for BTE approaches *in vivo* studies.

1. Introduction

Bone regeneration is an essential process following jawbone losses in volume and functionality, whether due to tumors, trauma, or loss of dental elements. To date, autologous bone grafting is considered the "gold standard" for jawbone regeneration [1-3]. However, despite its efficacy, this approach presents a spectrum of complications. The main challenges associated with autologous bone encompass the morbidity

* Corresponding author at: Department of Medical, Oral and Biotechnological Sciences, Center for Advanced Studies and Technology CAST, "G. d' Annunzio" University Chieti- Pescara, Via Luigi Polacchi 11, 66100 Chieti, Italy.
E-mail address: domitilla.mandatori@unich.it (D. Mandatori).
[1] Domitilla Mandatori and Emira D'Amico have equally contributed to this work.
[2] Michele Furlani and Letizia Penolazzi have equally contributed to this work.

https://doi.org/10.1016/j.jdent.2024.105411
Received 25 June 2024; Received in revised form 15 October 2024; Accepted 15 October 2024
Available online 18 October 2024

linked to the donor site, potential bleeding complications, chronic pain, and additional concerns like diminished graft vascularization and heightened resorption rates in the post-operative phase. Addressing these multiple issues is critical to promote advancements in the field of bone grafting for jaw reconstruction and enhancing patient outcomes. In this context, a crucial aspect to highlight is the employment of specialized scaffolds developed exploiting bone-substitute biomaterials that include inorganic or organic, natural, or synthetic materials. Various studies have underscored that scaffolds should not be perceived solely as structural frameworks aimed at mechanically replacing the natural bone extracellular matrix (ECM). Instead, they should be recognized as indispensable tools facilitating cell adhesion, proliferation, and differentiation, thereby orchestrating the subsequent development of new bone tissue [4].

In this regard, during three decades of in-depth research on biomaterials aiming at the creation of customized scaffolds as substitutes for autologous bone grafts, some authors have proposed and analyzed different materials and structural designs. Among these, the advantages of using hydroxyapatite (HA) and β-tricalcium phosphate (TCP) in the 30/70 mixture (HA/TCP) have been widely observed [5,6]. The success of this biomaterial fundamentally lies in its slow but reliable reabsorption, closely linked to the kinetics of the patient's bone turnover, which is further influenced by the mechanical stimuli received. In this context, vessels' spatial distribution has great impact within the bioengineered bone substitutes [7]. Indeed, it is well known that vascularization is one of the most crucial challenges in bone tissue engineering, as diffusion of nutrients and oxygen, along with waste exchange, is required to support osseointegration and osteogenesis during bone healing and regeneration processes: if cells are >100–200 μm far from the nearest blood vessel, they die due to lack of oxygen and nutrients [8,9]. However, to date, efforts to create vascularized bone substitutes *in vitro* are not satisfactory, and effective application of tissue-engineered vascularized bone grafts in clinical cases of large bone defects is very limited [6,10,11].

Moreover, scaffold pore sizes are well known to be crucial parameters for tissue ingrowth and vascularization, as high porosity (total porosity > 50 %) and large pores may enhance bone ingrowth and integration of the biomaterial. Based on the early investigations, the minimum recommended pore size for a scaffold is 100 μm. However, subsequent studies have shown that a porous sizes in the range of 300 to 400 μm could improve bone tissue formation [12-14].

In this context, we have widely shown, by *in vitro* and *in vivo* studies, that customized HA/TCP, produced by three-dimensional (3D) printing and with a 3D grid-like structure, is highly reminiscent of cancellous porous structure. Moreover, we have also demonstrated that, from 5 to 6 months after grafting, it exhibits good performances both in terms of bone regeneration and vascularization of non-critical oral bone defects [11,15]. Our previous studies allowed also to validate novel diagnostic tools, like the use of synchrotron phase tomography for simultaneous 3D imaging and quantitative analyses of microvascularization and bone microstructure [7,16,17].

However, in the case of critical (large) bone defects [18], the presence of a porous structure may be insufficient to achieve the total vascularization of the graft; thus, the production of engineered large vascularized 3D constructs is still a critical challenge.

Therefore, in recent years, awareness has grown of the need to develop *in vitro* systems that replicate, as faithfully as possible, the characteristics of the tissue microenvironment of the jawbone [19]. This has a dual objective, namely an in-depth knowledge of the jaw biological environment, associated with the development of effective therapeutic approaches in case of large bone defects. This is a major current challenge in regenerative dentistry, especially in bone tissue engineering (BTE) approaches aimed at repairing damaged bone tissue, caused by either bone tumor resection, traumatic injury, or congenital malformation [20]. However, the response of the tissue microenvironment to bone repair scaffold implantation in the defect area, is not always so predictable. This unpredictability can be due to several reasons, including patient characteristics and local adverse events, such as inflammation or infection [21]. Therefore, BTE is encouraged to consider patient-specific and trauma-specific parameters to achieve the production of tailored scaffolds inspired by the principle of "personalized medicine", as reported in recent reviews [22-24]. Aiming at this purpose requires careful study on how to replicate and optimize the *in vivo* jawbone microenvironment using *ex vivo* and/or *in vitro* models. Therefore, nowadays, research is defining *in vitro* preclinical validation platforms where scaffolds under exam aspire to provide a 3D system combining bone-forming cells (osteoblasts), bone-resorbing cells (osteoclasts), and vascular cells (endothelial cells) [25]. The main purpose of this setup is to generate a 3D structure with a spatial organization that replicates the cell-cell and cell-matrix interactions together with the different biochemical signals, useful to evaluate the potential of a given scaffold. In this respect the choice of cell source able to mimic the bone microenvironment is therefore crucial. Bone cells isolated from different skeletal sites (and embryonic layers) show different proliferation rate, ability to mineral matrix deposition and, not least, angiogenic activity (VEGF secretion) [26].

In accordance with these principles, the present study focuses on a biphasic calcium phosphate (BCP) scaffold printed with an advanced robocasting method. The objective is to evaluate scaffold properties and behavior when human osteoblasts, osteoclasts, and vascular cells are seeded on it. Indeed, BCP bioceramics, created by blending and sintering non-resorbable HA [$Ca_{10}(PO_4)_6(OH)_2$] with resorbable TCP [$Ca_3(PO_4)_2$] [27,28], represent highly suitable material for synthetic oral bone substitutes since HA provides a stable scaffold for new bone formation through both its osteoconduction and osteoinduction properties. In addition, the dissolution of β-TCP oversaturates the local environment with Ca^{2+} and PO_4^{3-} ions, thereby expediting the induction of bone formation within the porous spaces of the biphasic constructs [29].

Based on these assumptions, herein we developed an innovative BCP 3D scaffold, characterized by a greater definition of macro- and microscopic details as projected by computer-aided design (CAD). Interestingly, the BCP scaffold structure was designed with defined micro-sized channels and in larger interconnected pores (>300 μm) to aid and potentially guide both the osteo- and angiogenic process [14,30]. The innovative printing method is capable of creating curved struts, which are expected to significantly enhance biomechanical performance. This allows for the formation of large pores, leading to an improved biological invasion of even structures with a greater volume. Taking these considerations into account and aiming to mimic the characteristics of a jaw tissue microenvironment, this study aimed to evaluate the impact of the BCP scaffold on both bone-derived and vascular cells. The focus was on promoting both bone tissue regeneration and new blood vessel formation, which are essential in presence of a large bone defect. Therefore, we employed a novel triculture system, previously unused, where primary human osteoblast, human monocytes (as osteoclast precursors), and endothelial cells were seeded onto the BCP scaffold.

This study aims to investigate the influence of the BCP scaffold on the behavior of cells from different origins. Additionally, it highlights the advantages and limitations of a 3D *in vitro* bone model as a platform for designing and testing effective oral bone tissue (BTE) approaches, as well as for evaluating regenerative therapies in dentistry.

2. Materials and methods

2.1. BCP scaffold production

The ceramic scaffolds used in this study were fabricated by direct rapid prototyping technique dispense-plotting (RePore, Biomed Center, Innovation gGmbH, Bayreuth, Germany), similar to robocasting but deploying a rheometrically defined slurry and much finer needle diameter [31]. A virtual scaffold model was designed with a cylindrical outer geometry by using 3D CAD software (SolidEdge, Siemens PLM Software). The size of the model was adapted to the shrinkage of the

ceramic material in the subsequent sintering process. The inner geometry, *i.e.*, the pathway of the material rods, was defined by custom-made software that generates the control commands of the rapid prototyping machine. To build up the green bodies, material rods consisting of a paste-like aqueous ceramic slurry were extruded from a cartridge through a nozzle and deposited using an industrial robot (GLT Pforzheim, Germany). A micro-stepping displacement control unit was used. In this study, HA and TCP powders (Merck, Germany) were blended to get a biphasic powder mixture with a HA/TCP weight ratio of 30/70. The characteristic rheological behaviour of the aqueous biphasic ceramic slurry was achieved by thermal treatment of the raw powder at 900 °C for 1 hour and by adding a compatible binder/dispersant system of organic additives of 10.5 wt percentage (wt.%) relative to the mass of ceramic powder. The rod deposition was controlled in x, y, and z directions to assemble 5 mm x 5 mm x 5 mm cubic scaffolds layer by layer on a building platform. By rotating the direction of the rod deposition by 90° from layer to layer a 3D network with an interconnected pore structure was generated. The assemblies made of ceramic slurry were dried at room temperature and subsequently sintered with a stepwise heat increase to remove the organics, holding for 30 min at 420 °C, then increasing to sinter at 1250 °C for 1 h By preparing the slurry homogeneously without aggregates larger than 100 μm and free of air bubbles, a 0.22 μm needle was used, allowing for exact control of the rim and pores even in these small dimensions.

2.2. BCP scaffold imaging methods

The top and lateral sides of BCP scaffolds were studied by Tescan VEGA3 (Tescan Company, Brno, Czech Republic) scanning electron microscope (SEM). SEM micrographs of fractured surfaces were also acquired after the mechanical compression test.

X-ray micro-computed tomography (XμCT) analyses were performed by a Bruker Skyscan 1174 system (Bruker, Kontich, Belgium), to verify the 3D structure geometrical accuracy and the presence of (eventual) residual powder. Projections were obtained with the following experimental parameters: X-ray tube voltage = 50 kV; cathode current = 800 μA; pixel size = 6.5 μm; total rotation angle = 180°; rotation step = 0.4°; exposure time per projection = 10 s; aluminum (Al) filter thickness = 1 mm. Projections were processed in stacks of cross-sectional slices by the SkyScan reconstruction program NRecon (v. 1.10.6.2, Bruker, Kontich, Belgium) under the following conditions: smoothing = 3; ring artifacts reduction = 7; beam hardening correction = 70 %. The 3D models of the BCP scaffolds were obtained by the SkyScan CT-Vox software (v. 3.3.0, Bruker, Kontich, Belgium).

2.3. BCP scaffold mechanical tests

The mechanical performance of the BCP scaffolds was investigated by uniaxial compressive tests in 5 × 5 × 5 mm^3 samples. A SkyScan Material Testing Stage coupled to the 1174 X-ray microtomographic system was employed with the following characteristics: maximum compression force of 440 N, displacement sensor accuracy of ± 0.01 mm, load measurement accuracy of ± 4 N (± 1 % of the full range), and maximum object diameter and height (in compression mode) of 20 mm and 23 mm, respectively.

2.4. Human osteoblasts

Human osteoblasts (hOBs) were obtained from vertebral lamina samples discarded during spinal surgery to remove the lumbar herniated disc. Bone fragments were obtained from 3 donors ($n = 3$; mean age 34 years, 2 males and 1 female, Pfirrmann grade 3–4) using research protocol approved by the Ethics Committee of the S. Anna Hospital (protocol no 160,998, approved on November 17th, 2016). Briefly, bone fragments were placed in sterile phosphate-buffered solution (PBS) at 4 °C and dissected within 16 h after removal. From each patient, with no comorbidity, bone chips were minced into smaller pieces, as previously reported [32] washed twice with PBS, plated in T-25 culture flasks (Sarstedt, Nümbrecht, Germany), and cultured in 50 % DMEM high-glucose/50 % Ham's F12, supplemented with 10 % FCS, 1 mM l-Glutamine, antibiotics (penicillin 100 μg/mL and streptomycin 10 μg/mL). Upon detection of a cell colony from the bone fragments (after 7 days), the cells were expanded until confluent (passage zero, P0). The cells were then harvested after treatment with 0.05 % trypsin ethylenediamine tetraacetic acid (Sigma-Aldrich), washed, counted by hemocytometric analysis, and used for further experiments (passage 1 to passage 3). During the culture period, cells were incubated at 37 °C in a humidified atmosphere of 5 % CO_2, and the medium was changed every 3 days. For osteogenic differentiation, hOBs were cultured for up to 14 days in an osteogenic medium (OM) consisting of DMEM high-glucose 10 % FCS, 10 mM β-glycerophosphate, 100 nM dexamethasone, and 100 μM ascorbate.

2.5. Human monocytes

Human monocytes (hMCs), as osteoclasts precursors were isolated from the human peripheral blood (PB) of four healthy donors ($n = 4$, 2 males and 2 females, median age 46) after informed consent (protocol no 0,110,952, approved on November 30th, 2015) by using sequential density gradient centrifugations over Ficoll (Merck KGaA) solution. hMCs were then cultured in basal medium (DMEM high-glucose supplemented with 10 % FCS, 1 mM l-Glutamine, penicillin 100 μg/mL and streptomycin 10 μg/mL) until seeding on BCP scaffolds.

2.6. Human umbilical vein endothelial cells

Human umbilical vein endothelial cells (HUVECs) were isolated from umbilical cords collected immediately after delivery (36–40th gw) from randomly selected healthy Caucasian mothers at the Hospital of Chieti and Pescara (Italy). All procedures adhered to the ethical standards of the Institutional Committee on Human Experimentation (Protocol no.: 1879/09COET) and with the Declaration of Helsinki Principles. Signed informed consent was obtained from each participating subject. In detail, after perfusion of umbilical vein cords with 1 mg/mL of Collagenase 1A at 37 °C, explanted HUVECs were grown in 1.5 % gelatin-coated tissue culture plates in endothelial growth medium (EGM) composed of DMEM/M199 (1:1) added with 1 % l-glutamine, 1 % Penicillin-Streptomycin, 20 % FBS, 10 μg/ml heparin and 50 μg/ml Endothelial Cell Growth Factor. For the experiments, HUVECs between the third and fifth passages were used. For cellular visualization, 4×10^5 HUVECs were treated with 5 mM CellTracker ™ Green CMFDA (Thermo Fisher Scientific, Waltham, MA USA) for 30 min, trypsinized, and seeded on a BCP scaffold. After 4 days, samples were observed under a fluorescence microscope (Nikon, Optiphot-2; Nikon Corporation, Tokyo, Japan) using the filter block for fluorescein.

2.7. BCP scaffold seeding and cell culture

Once the BCP scaffold was manufactured, bone and vascular cells were seeded on it to study its biological behavior, following the experimental plan shown in Fig. 1 and described below.

In the first experimental group (BCP+hOBs/hMCs; $n = 3$), hOBs and hMCs were seeded on a BCP scaffold pre-soaked in basal medium (10 min). In detail, 5×10^4 hOBs were previously seeded, and after 24 h (time 0), 5×10^4 hMCs were added to the scaffold. Then, hOBs and hMCs were co-cultured in OM for up to 14 days (Fig. 1a).

In the second group (BCP+HUVECs; $n = 3$) only vascular cells were employed. BCP scaffolds were pre-soaked in gelatin 1.5 % solution for 10 min (37 °C) and seeded with 2×10^5 HUVECs cultured in EGM for up to 7 days (Fig. 1b).

For the tri-culture system (third experimental group; BCP+hOBs/hMCs/HUVECs; $n = 3$), HUVECs were seeded 2×10^5 on 1.5 % gelatin-

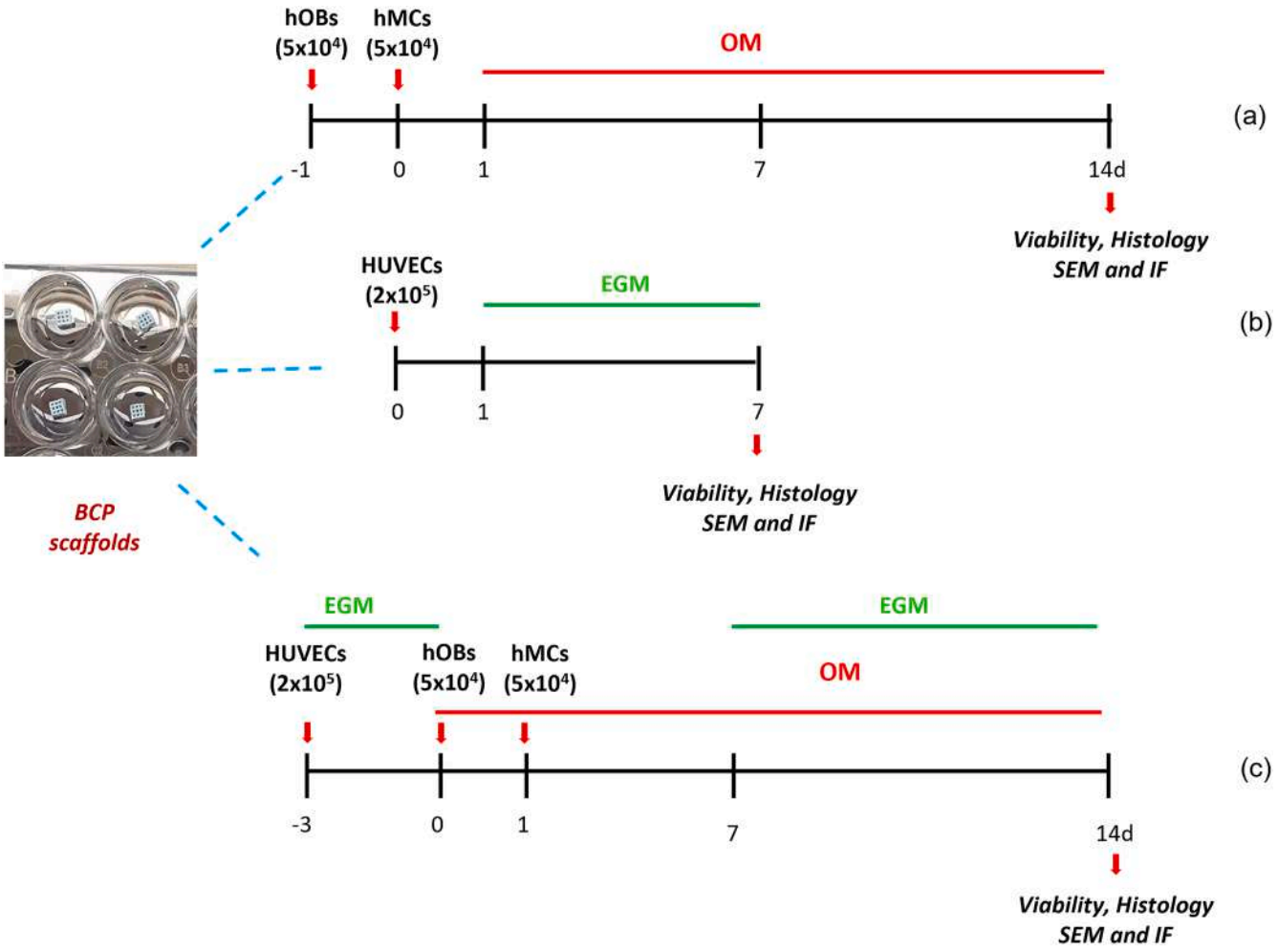

Fig. 1. Experimental plan for culturing human osteoblasts (hOBs), human monocytes (hMCs), and human umbilical vein endothelial cells (HUVECs) seeded on biphasic calcium phosphate (BCP) scaffold. The three following experimental group were set up: **a** hOBs (5×10^4) and hMCs (5×10^4) seeded and co-cultured on BCP scaffold for up to 14 days in osteogenic medium (OM) (BCP+hOBs/hMCs); **b** HUVECs (2×10^5) seeded and cultured on BCP scaffold for up to 7 days in endothelial growth medium (EGM) (BCP+HUVECs); **c** hOBs (5×10^4), hMCs (5×10^4), and HUVECs (2×10^5) seeded and cultured on BCP scaffold for up to 14 days in OM and EGM (BCP+hOBs/hMCs/HUVECs). Each experimental group was analyzed in biological triplicates ($n = 3$). Scanning electron microscopy (SEM), immunofluorescence (IF).

coated BCP scaffold and cultured in EGM. After 72 h, 5×10^4 hOBs were added and EGM was changed to OM. After a further 24 h also 5×10^4 hMCs were seeded on BCP scaffold and cultured for up to 14 days (Fig. 1c).

Preliminary experiment has been performed to determine the best cell seeding densities and the timeline of the co-culture system (Fig. Supplementary 1)

2.8. Cell-engineered BCP scaffold characterization by scanning electron microscopy (SEM)

Cell adhesion and morphology were investigated by SEM analyses. Specifically, the BCP scaffold with cultured cells was fixed with a solution of 3.5 % glutaraldehyde in 0.1 M sodium cacodylate buffer ($C_2H_6AsO_2$ Na) and kept at a temperature of 4 °C. Afterward, samples were post-fixed with 2 % OsO4, washed in distilled water, dehydrated with ascending series of alcohol, and finally immersed in hexamethyldisilazane and dried in a desiccator to air-dry at room temperature. Dried samples were subsequently mounted to aluminium stubs using double-sided carbon tapes, coated with a layer of gold (150 Å) using the DSR1 desk sputter coater, and observed under the Phenom XL (Alfatest, Cernusco sul Naviglio, Italy) microscope at various magnification.

2.9. Cell viability

Cell viability cultured on the BCP scaffold was determined by a live/dead cell imaging protocol, as previously described [33]. After staining with propidium iodide (PI) and Calcein-AM, cells were imaged by a fluorescence microscope (Nikon, Optiphot-2, Nikon Corporation, Japan) using the specific filter blocks. Dead cells were stained in red, whereas viable ones were in green.

2.10. Histological and immunofluorescence analyses

The BCP scaffold with cultured cells was fixed with 10 % buffered formalin (Sigma Aldrich, St Louis, Missouri, USA) and then dehydrated in an ascending series of alcohol. Thereafter, samples were embedded in glycol-methacrylate resin (Technovit 7200 VLC; Kulzer, Wehrheim, Germany) and sectioned with a high-precision diamond disk at about 100 μm. The obtained slices were stained with acid fuchsin and toluidine blue and observed using a light microscope (Laborlux S, Leitz, Wetzlar, Germany) connected to a high-resolution video camera (3CCD, JVCKY-F55B, JVC, Yokohama, Japan) and interfaced with a monitor connected to a computer. Images were taken at the magnification of 40x and 100x.

Slices previously stained for histological analyses were bleached by abrasion with sandpaper and then processed for immunofluorescence

(IF) analyses. In detail, following a permeabilization step with a Triton 0.1 % solution, slices were incubated with the following primary antibodies: anti-CD31 (EPR3094), anti-alkaline phosphatase (ALP; PA5–47,419, ThermoFisher Scientific, Waltham, MA, United States) and anti-TRAP (PA5–116,970, ThermoFisher Scientific, Waltham, MA, United States). Anti-goat Alexa Fluor 488 (A11055, ThermoFisher Scientific, Waltham, MA, United States) and anti-rabbit Cyanine 3 (A10520, ThermoFisher Scientific, Waltham, MA, United States) were used as secondary antibodies.

Nuclei were stained with 4′,6-diamidino-2-phenylindole (DAPI), and images were taken using a confocal microscope (Zeiss LSM-800, Carl Zeiss Meditec AG, Oberkochen, Germany).

2.11. Statistical analyses

The statistical analyses of the data were performed with the software package Prism 6.0 (GraphPad Software, San Diego, CA, United States). All data were presented as mean ± standard deviation (SD). Statistical significance in mechanical tests between Top Load and Lateral Load groups was evaluated by Student's *t*-test. Statistical significance was set at $p < 0.05$.

3. Results

3.1. BCP scaffold morphometric characterization

Scaffolds were investigated by XμCT (Fig. 2, panel a), obtaining the morphometric data listed in Fig. 2– right side. It was found that the volume percentages of the biomaterial (Str.Vol%) and porosity (Por.Vol %) are very similar, 46 ± 11 % *vs*. 54 ± 11 %, respectively. Indeed, also the mean strut thickness (Str.Th) is dimensionally like the mean pore thickness (Por. Th), 585 ± 118 μm *vs*. 719 ± 49 μm, respectively. Moreover, the anisotropy degree of the biomaterial structure (Str.DA) and the anisotropy degree of the porosity network (Por.DA) were also evaluated. These indices measure the similarity of the biomaterial structure or the porosity network to a uniform distribution and vary from 0, corresponding to the perfect isotropy, to 1, indicating all struts or pores confined to a single plane or axis. It was found that both Str.DA and Por.DA were similar (0.328 ± 0.037 *vs*. 0.339 ± 0.021 respectively) but not equal to 0, suggesting that a small anisotropy was present. Furthermore, the fractal dimension of the biomaterial structure (Str. FrD) was also assessed. Str.FrD parameter indicates the extent to which an irregular structure tends to fill space at different scales. We found a very low value (2.051 ± 0.017: range 2–3), suggesting that the structure is extremely regular. Finally, the interconnectivity of struts (Str.ConnD – mm^{-3}) and pores (Por.ConnD – mm^{-3}) were analyzed: their high values, 1.88 ± 0.14 mm^{-3} for Str.ConnD and 1.90 ± 0.12 mm^{-3} for Por.ConnD. indicated the presence of entangled struts and well-connected pores.

SEM observations and 2D cross-sectional slice from XμCT showed that the top faces of the samples (Fig. 2, panels b and d, respectively) have a morphology, in terms of architecture and porosity, completely different with respect to lateral faces (Fig. 2, panels c and e, respectively). However, we assessed through the same techniques that adjacent lateral faces of scaffolds were identical from a morphological and morphometric point of view. Thus, adjacent lateral faces were assumed to respond with indistinguishable behaviour once submitted to the same applied load, during the mechanical compression tests carried out.

3.2. BCP scaffold mechanical tests

Six BCP scaffolds were tested by uniaxial compressive test on the longitudinal direction (top load), and six identical BCP scaffolds were tested by uniaxial compressive test on the transversal one (lateral load). For both directions, the results of compressive tests were plotted as a stress/strain curve, from which the following parameters were extracted: (1) yield strength point (MPa), (2) ultimate strength point (MPa), and (3) fracture point (MPa). In order to compute the stress, effective areas of both top and lateral faces were calculated using the ImageJ software (NIH, USA ImageJ software, public domain available at: http://rsb.info.nih.gov/nih-image, v. 1.53q). The effective areas were obtained considering the real contact surfaces, *i.e.*, subtracting any surface porosity in five contiguous slices obtained from the XμCT reconstructions, in both the longitudinal and the transversal faces.

Using the same protocol tested in a previous study [5], values of stress (MPa) and strain (%) were measured in the yield, in the ultimate, and in the fracture points, obtained from mechanical compression test on top and lateral sides (Fig. 3). In particular, the strength values at the yield, ultimate, and fracture points obtained from mechanical compression tests on the top and lateral side, were reported in Fig. 3 bottom table.

The strength values obtained in the top direction were more than twice as high as those in the lateral direction, with always significant

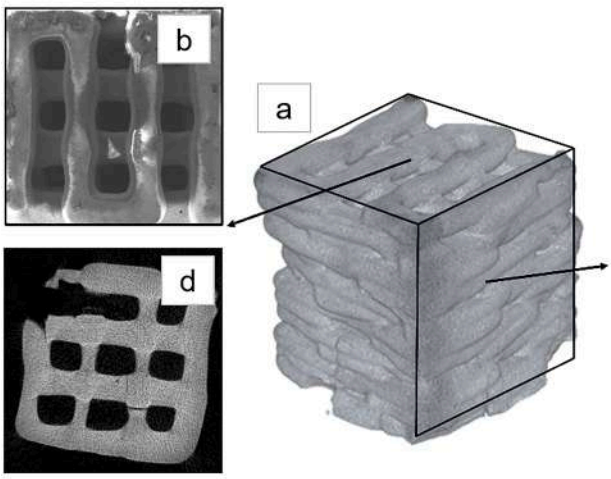

Parameters	Mean ± SD
Str.Vol%	46 ± 11 %
Por.Vol%	54 ± 11 %
Str.Th	585 ± 118 μm
Por.Th	719 ± 49 μm
Str.DA	.328 ± .037
Por.DA	.339 ± .021
Str.FrD	2.051 ± .017
Str.ConnD	1.88 ± .14 mm^{-3}
Por.ConnD	1.90 ± .12 mm^{-3}

Fig. 2. Morphometric characterization of the BCP scaffold. a Three-dimensional (3D) model of the BCP scaffold through X-ray micro-computed tomography (XμCT), with **b-d** top faces and **c-e** lateral faces showing different patterns; **b-c** SEM micrographs; **d-e** single slices of XμCT reconstructions; (right panel) XμCT data.

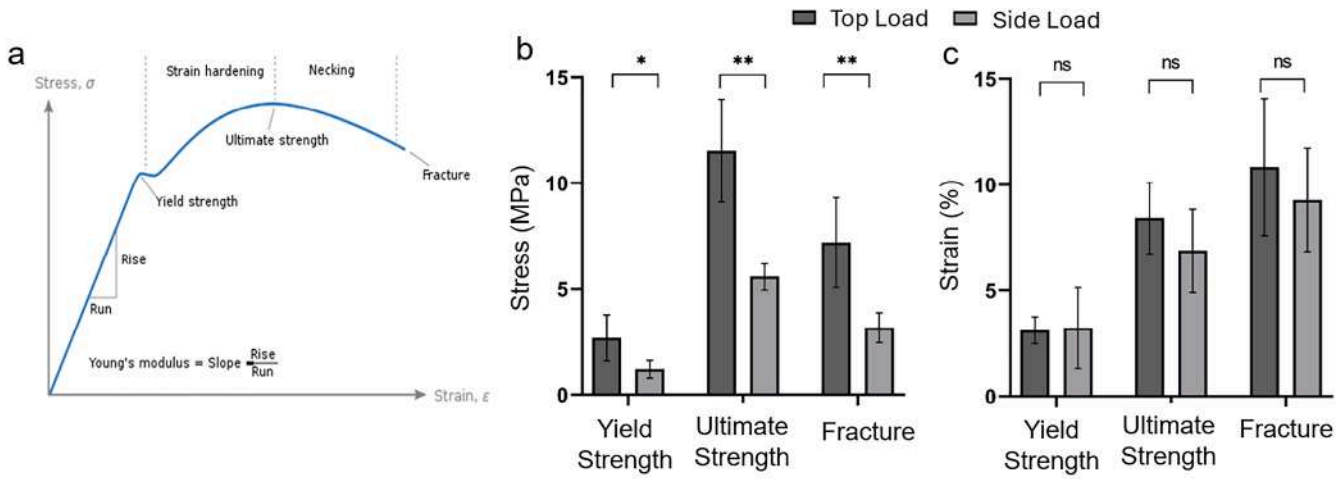

Parameters	Yield strength	Ultimate strength	fracture
top side	2.7 ± 1.1 MPa	11.5 ± 2.4 MPa	7.2 ± 2.1 MPa
lateral side	1.2 ± 0.4 MPa	5.6 ± 0.6 MPa	3.2 ± 0.7 MPa

Fig. 3. Mechanical Testing of the BCP scaffold. a Benchmark Stress-Strain curve with the considered relevant points, **b** Histograms of observed stress and **c** strain in both the top and lateral side load tests. Asterisks indicate statistically significant differences between top and lateral side groups, $*p < 0.05$, $**p < 0.01$; (bottom table) Mechanical compression test on top and lateral sides. Values of yield strength (MPa), ultimate strength (MPa), and fracture strength (MPa) were reported as mean ± standard deviation (SD).

differences. Conversely, the strain values were similar in both loading directions.

Afterward, the fracture areas were investigated in all 12 samples by both XμCT and SEM: the analyses, at different magnifications, showed that the BCP scaffolds presented fracture only in the rods and not in the nodes. At high magnification, it was observed the presence of micropores in the fracture surfaces (Fig. 4).

3.3. Bone cell (hOBs and hMCs) adhesion on BCP scaffold

Once the mechanical properties of the BCP scaffold were characterized, its ability to allow bone cell adhesion was examined following the experimental set up reported in Fig. 1. Following preliminary experiments to determine the best cell seeding densities and the timeline of the co-culture system (Fig. S1), hOBs and hMCs were co-cultured at a 1:1 ratio (5×10^4 each) on the BCP scaffold for 14 days. SEM analyses demonstrated the ability of bone cells to adhere to the scaffold surface (Fig. 5a).

This observation was corroborated by Calcein AM/PI staining and histological analyses, indicating that the seeded cells were viable and effectively covered all areas of the BCP scaffold, with notable growth on its outskirts (Fig. 5b and 5c, respectively). Furthermore, the ability of the BCP scaffold to preserve cellular native phenotype over time was verified by IF analyses. Indeed, after 14 days of culturing in OM, cells positive for TRAP and ALP were observed, suggesting the presence of mature and healthy osteoclasts and osteoblasts, respectively (Fig. 5d).

3.4. HUVECs adhesion on the BCP scaffold

HUVECs were seeded on the BCP scaffold to elucidate whether the scaffold supports not only the adhesion of bone-derived cells but also the adhesion and growth of vascular ones. Specifically, HUVECs were seeded and cultured for up to 7 days on a BCP scaffold pre-soaked in 1.5 % gelatin. As shown in Fig. 6, cells were viable (6a) and able to maintain their spindle shape morphology (6b). Furthermore, SEM and IF analyses also revealed the presence of adherent HUVECs expressing the vascular-specific marker CD31 on the BCP scaffold surface (Fig. 6c and d).

3.5. Tri-culture (hOBs, hMCs, and HUVECs) on the BCP scaffold

After confirming the capability of bone-derived cells (hOBs and hMCs) and vascular cells (HUVECs) to adhere to the BCP scaffold, a 3D human tri-culture system incorporating all three cell types was developed. The objective was to evaluate the influence of the BCP scaffold on cell behavior within a 3D system that closely mimics the jawbone microenvironment. Based on the previous results, HUVECs were seeded and cultured for 72 h on a BCP scaffold coated with 1.5 % gelatin. Following 24 and 48 h, 5×10^4 hOBs and hMCs were added, respectively. After 14 days of tri-culture, BCP scaffolds were completely covered with viable cells, apparently both in the outer and the inner regions of the scaffold (Fig. 7a). Furthermore, HUVECs were treated with CellTracker ™ Green CMFDA dye, enabling precise tracking of their location on the BCP scaffold. As reported in Fig. 7b, HUVECs mainly migrate in the scaffold porous network core, showing a tube-like disposition. Histological analyses obtained at 14 days of tri-culture, showed that HUVECs, hOBs, and hMCs covered one side of the scaffold (as indicated by the arrows in Fig. 8a), while the opposite side remained partially uncovered. Furthermore, at higher magnification, cell cordons were observed within the pores, and a dense layer of cells was noticeable.

Therefore, IF experiments were conducted to distinguish the three cell types. Fig. 8b illustrates that differentiated osteoclasts, HUVECs, and hOBs, stained for TRAP (red), CD31 (purple), and ALP (green) respectively, adhered to the BCP scaffold, specifically colocalizing together along the edges of the scaffold (MERGE image). It is noteworthy that after 14 days of culture, a significant number of HUVECs were observed, likely influenced by the presence of hOBs and hMCs. Finally, although SEM analyses did not allow to distinguish the three cell types in the tri-

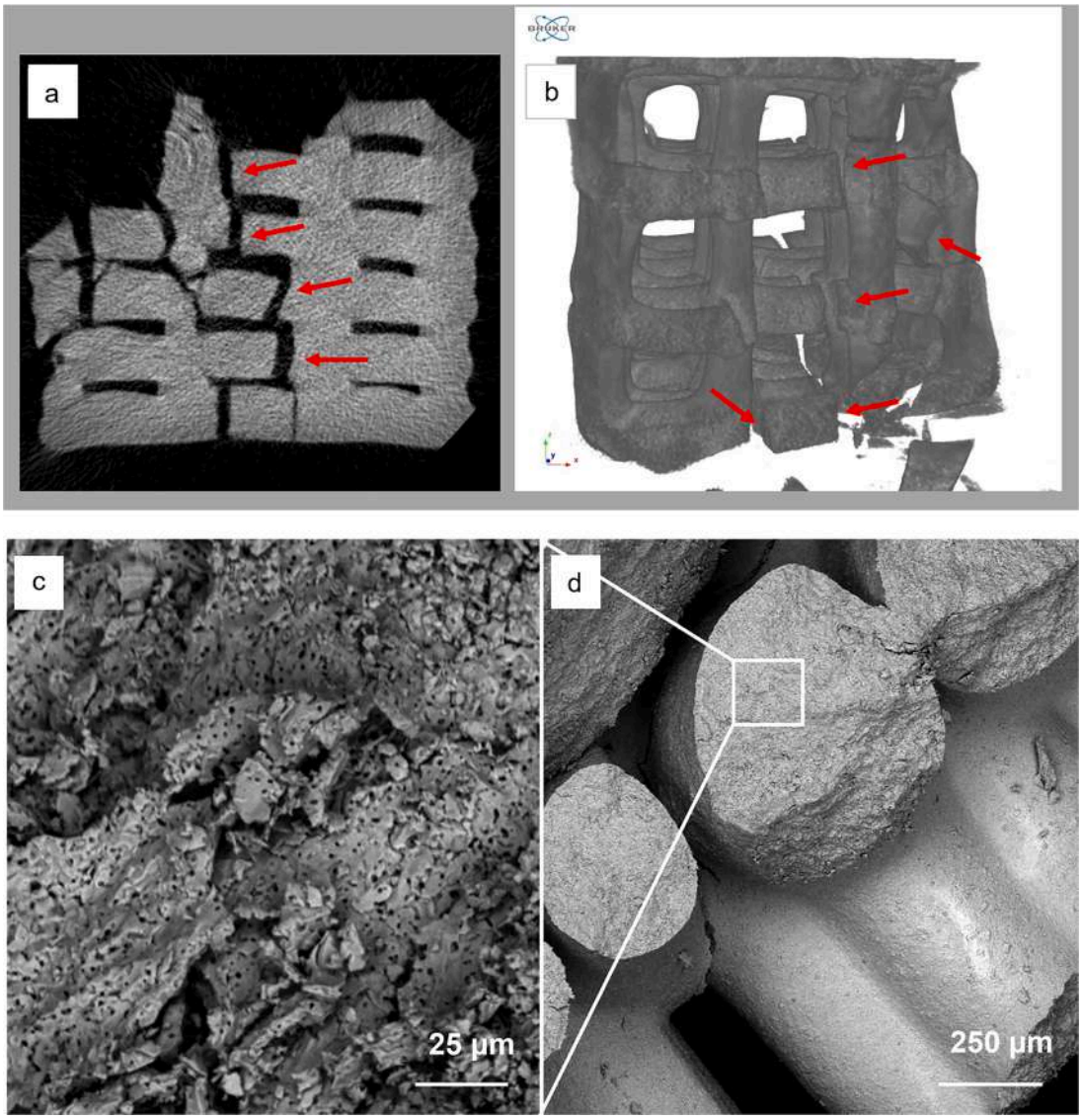

Fig. 4. Fracture imaging. XµCT showed that fracture occurred only in the rods and not in the nodes (red arrows): **a** two-dimensional (2D) slice; **b** 3D reconstruction; (**c**) Inset showing the fracture surface at higher magnification, highlighting the presence of micro-pores; **c-d** SEM observation of the fracture surface in a BCP scaffold fragment after mechanical compressive test.

culture system, images captured at different magnifications (Fig. 9a-c) unveiled substantial cell adhesion to the BCP scaffold, forming a prominent tissue-like cellular layer through interactive connections. Notably, SEM images also highlighted the presence of mineralized crystals within this tissue-like cellular layer. Energy-dispersive X-ray spectroscopy (EDX) analyses (Fig. 9d) confirmed that these crystals contained elements typical of the bone tissue mineral matrix, including calcium (Ca), phosphorus (P), oxygen (O), and carbon (C). This validates that the establishment of this tri-culture system effectively mimics the bone microenvironment.

4. Discussion

Currently, the main approach to addressing large oral bone defects involves the use of autologous bone graft. This procedure enhances spontaneous bone healing by providing an osteoconductive, osteoinductive, and/or osteogenic environment. However, it also presents several drawbacks, including the need for additional surgical procedures, a high risk of donor site morbidity, and limited availability of graft tissue [34,35].

For these reasons, there is growing interest in novel BTE approaches to stimulate the regeneration of large amounts of bone for repairing critical-sized defects. In this context, various guided bone regeneration (GBR) techniques have encountered complications, such as disturbed wound healing with a soft tissue dehiscence leading to a membrane exposure and often to subsequent infection of the bone graft [36]. To mitigate these complications and achieve sufficient regenerated bone volume, the custom-made computer-aided-design/computer-aided-manufacturing (CAD/CAM) procedure has been recently introduced. This method enables the production of 3D personalized scaffolds, offering clinicians ready-to-use solutions, tailored according to specific criteria such as the type and size of the bone defect [37]. Indeed, personalized scaffolds featuring a porous network that mimics the ECM promote and enhance bone tissue regeneration processes [38]. Nowadays, various scaffolds made from biomaterials including ceramics, bioactive glass compositions, collagen, and polymers have been tested to ensure specific mechanical properties of substrates [39], enabling clinicians to achieve safe and predictable short- and long-term outcomes [40]. Additionally, the use of cell-based scaffolds has shown promising results in BTE approach, especially in the oral field [41,42].

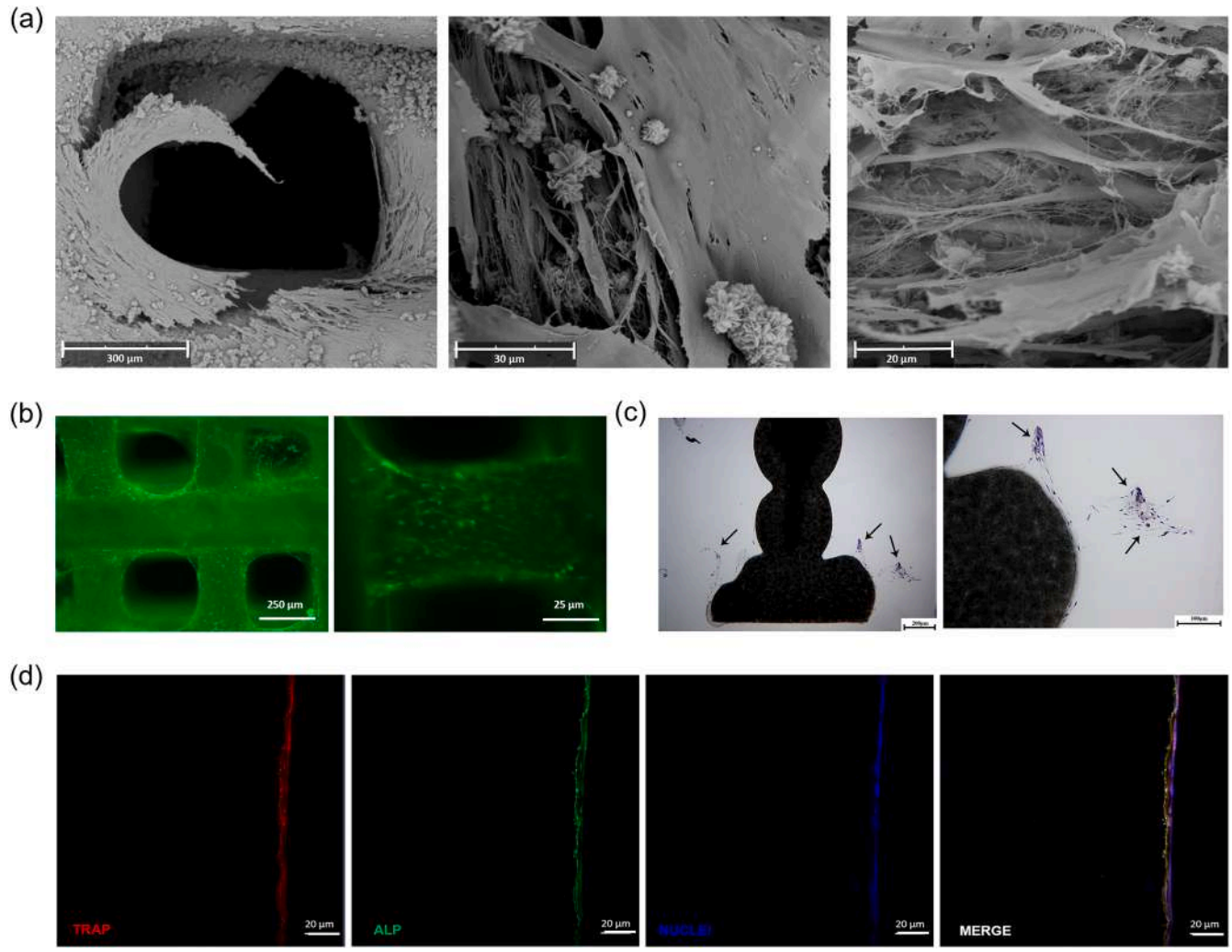

Fig. 5. hOBs/hMCs cultured on the BCP scaffold. a SEM images showing cell adhesion and distribution; **b** cell viability performed by Calcein-AM/Propidium Iodide (PI) double staining. Green fluorescence indicates the presence of Calcein-labeled live cells, while PI-labeled dead cells - red fluorescence - are undetectable; **c** Histological analyses performed by acid fuchsine and toluidine blue staining, and **d** expression of TRAP (red staining) and ALP (green staining) evaluated by IF analyses. Cells nuclei were stained in blue with DAPI.

Based on this assumption, this study combined a 3D printing CAD/CAM approach with an optimized mixture of 30 % HA and 70 % TCP, used as a base for the slurry, to develop an innovative BCP scaffold for regenerative purposes in dentistry. Then, to create a 3D cell model mimicking the oral microenvironment, the BCP scaffold was combined with primary cultures of hOBs, hMCs and HUVECs.

The slurry characteristics were improved by grinding and classing to achieve a finer slurry, allowing for more intricate details to be realized. As observed by both SEM and XμCT analyses, the manufacturing technique allowed the creation of regular 3D structures with large internal interconnected pores (Por. Th. ≅ 700 μm) free from residual powder. Indeed, as an alternative to the air-pressure controlled printers used in a previous scaffold fabrication [5], a 3-axis robot was equipped with direct-displacement driven syringes. This allowed for more precise control of the geometry, resulting in an optimized 3D scaffold with regard to pore structure (*e.g.*, large and highly interconnected pores) and physicochemical properties (*e.g.*, surface chemistry, surface topography, degradability, and stiffness) [43]. Indeed, relatively larger scaffold pores (> 300 μm) favor direct osteogenesis, even on the presence of large critical bone defects, as they facilitate for vascularization and high oxygenation of the microenvironment [44].

The mechanical tests performed in this study demonstrated that the application of an uniaxial compressive test on the longitudinal direction (top load), which corresponds to the scaffold build direction, exhibited superior mechanical resistance. This was observed not only when compared to the lateral faces (side load) of the same samples but also in relation to laser light stereo-lithography-printed [5] and traditionally sintered BCP scaffolds with the same weight composition [45]. As a consequence, the BCP scaffolds produced using the current additive manufacturing process were shown to be highly performing, suggesting that clinicians should consider orienting the scaffold with the build direction parallel to the maximum load expected during use in service.

Another aspect explored in this research was the evaluation of the biological behavior of the proposed BCP scaffolds. In this respect, the potential application of BCP scaffold for oral bone regeneration raises several issues related to the complexity of bone, which is characterized by the simultaneous presence of different cell populations, including osteoblasts, osteoclasts, and bone lining cells [46]. Several studies have investigated the osteoconductive and osteoinductive properties of ceramic scaffolds using bone and mesenchymal stem cells [47,48]. For instance, a previous study aimed at evaluating the osteoinduction and osteoconduction properties of a BCP scaffold demonstrated a predominant osteoinductive effect compared to osteoconduction. Indeed, it was observed that the amount and distribution of newly formed bone decrease from the side of the scaffold in contact with native bone toward the bulk of the scaffold itself [49]. However, it is also essential to

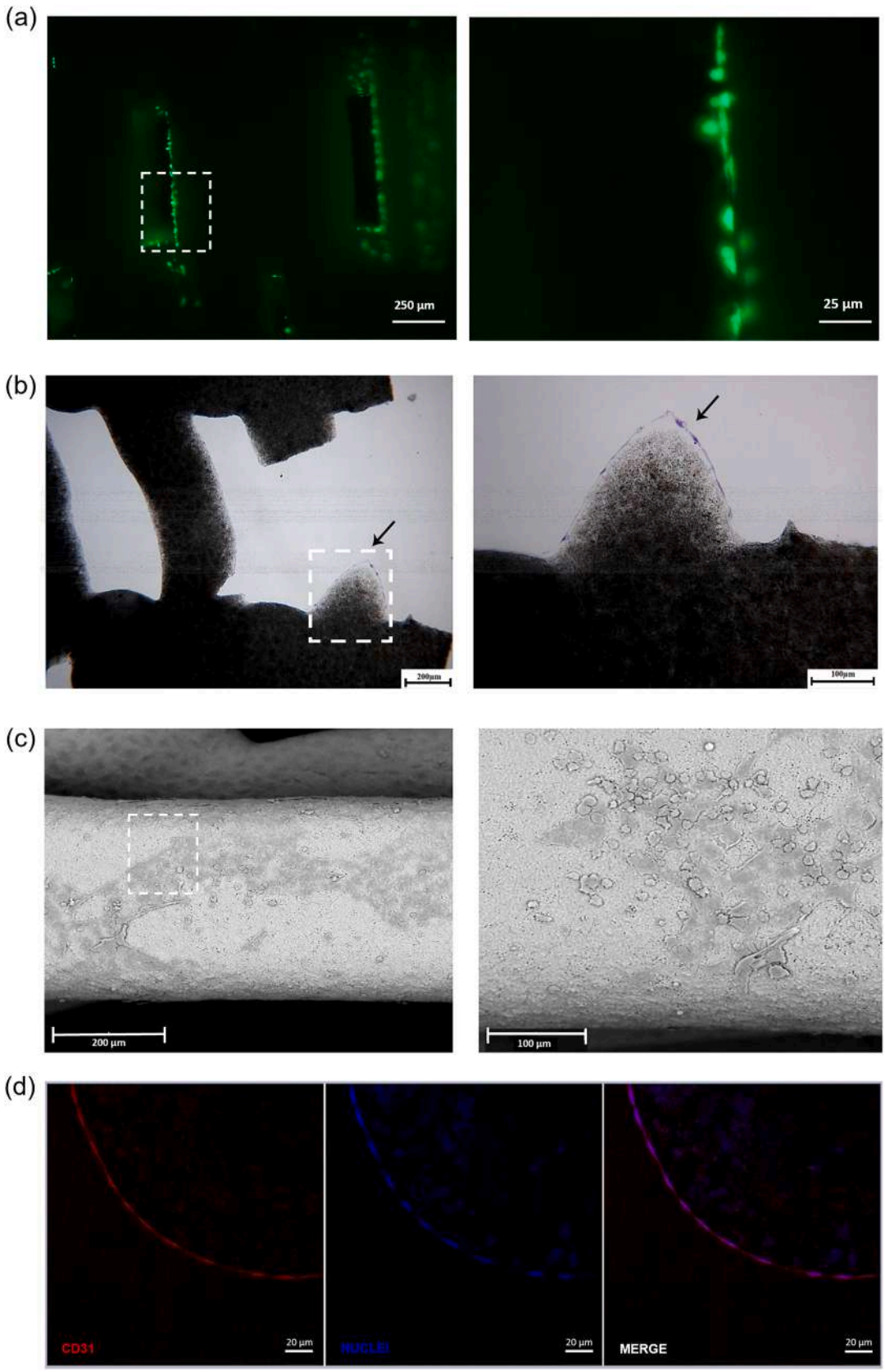

Fig. 6. HUVECs cultured on the BCP scaffold. a Cell viability performed by Calcein-AM/Propidium Iodide double staining. The green fluorescence indicates the presence of Calcein-labeled live cells, while PI-labeled dead cells - red fluorescence - are undetectable; **b** Histological analyses performed by acid fuchsine and toluidine blue staining, and **c** SEM images are reported. The square areas indicated by a dashed white line were shown at higher magnification on the right panels; **d** Expression of CD31 vascular marker (red staining) evaluated by IF analyses. Cells nuclei were stained in blue with DAPI.

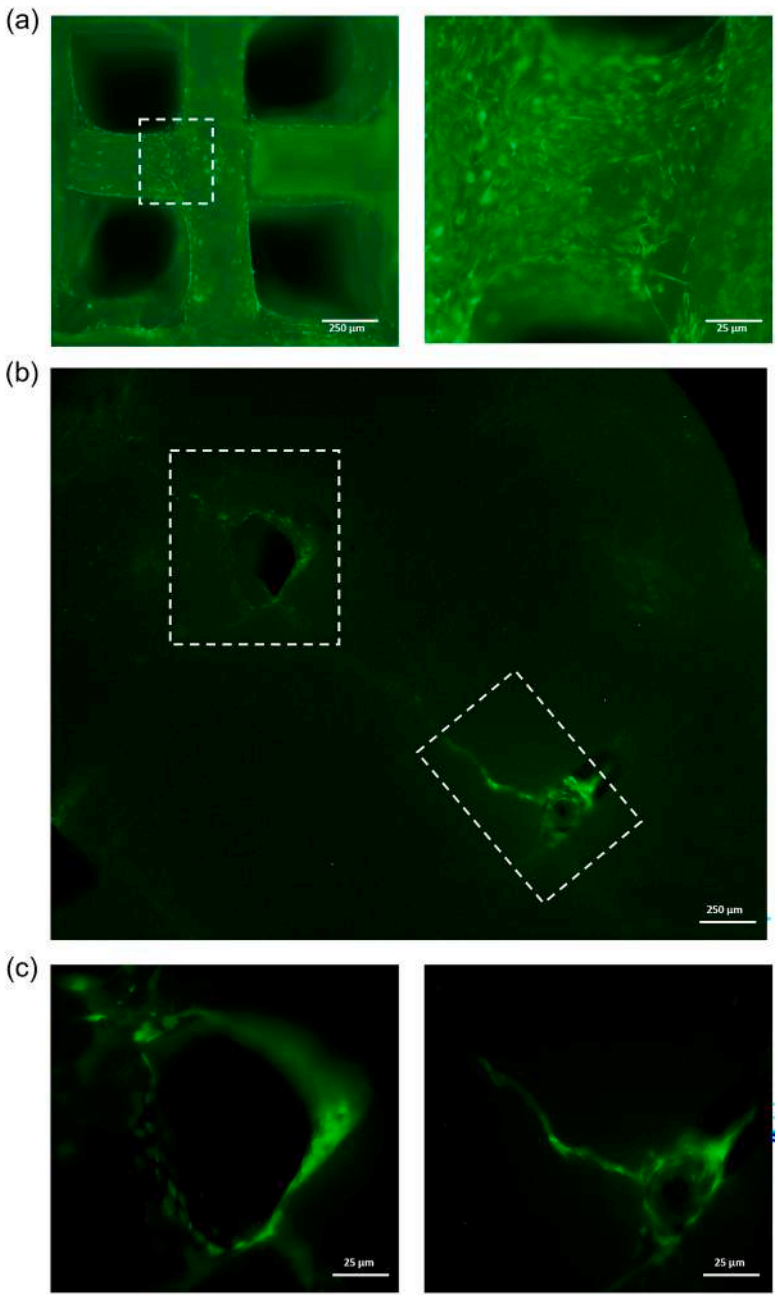

Fig. 7. hOBs/hMCs/HUVECs cultured on the BCP scaffold. a Cell viability determined by Calcein-AM/PI double staining; **b** fluorescently labeled HUVECs (CellTracker ™ green CMFDA) co-cultured with hOBs and hMCs and observed after 72 h. The green fluorescence indicates the presence of HUVECs on the BCP scaffold. High-magnification images were also reported (indicated by dashed square areas).

highlight the critical relationship between osteogenesis and angiogenesis for the successful application of BTE. This underscores the crucial importance of establishing a vascular network for effective bone regeneration, creating a positive feedback loop among osteoblasts, osteoclasts, and endothelial cells [50]. Indeed, while osteoblasts and osteoclasts contribute to maintaining a healthy bone remodeling process by balancing the production of mineralized osteoid matrix and bone resorption, endothelial cells play a vital role in the formation of a vascular network. This latter facilitates the exchange of nutrients, oxygen, and waste within the bone, ensuring cell survival and bone homeostasis [51]. Therefore, developing 3D scaffolds that effectively guide bone tissue regeneration simultaneously promoting osteogenesis and vasculogenesis remains a significant and challenging objective for researchers. Numerous studies have focused on creating *in vitro* and *ex vivo* systems that incorporate endothelial cell cultures [52,53]. However, to the best of our knowledge, no research has yet evaluated the biological behavior of a ceramic scaffold using a tri-culture system characterized by the simultaneous presence of osteoblasts, osteoclasts, and endothelial cells. Thus, our study established a triple culture model where primary hOBs, hMCs as osteoclast precursors, and HUVECs were seeded onto a novel BCP scaffold. The addition of primary vascular cells alongside bone-derived cells provides a significant advantage in developing a 3D model that closely mimics the *in vivo* microenvironment of a regenerative dentistry scenario.

In this study, the presence of viable cells and tissue-like cell layers after 14 days of tri-culture confirmed the osteoconductive properties of our BCP scaffold. Although SEM images did not allow us to distinguish among the three cell types, they clearly revealed significant cell adhesion to the BCP scaffold. This adhesion led to the formation of a remarkable tissue-like cell layer through interactive connections,

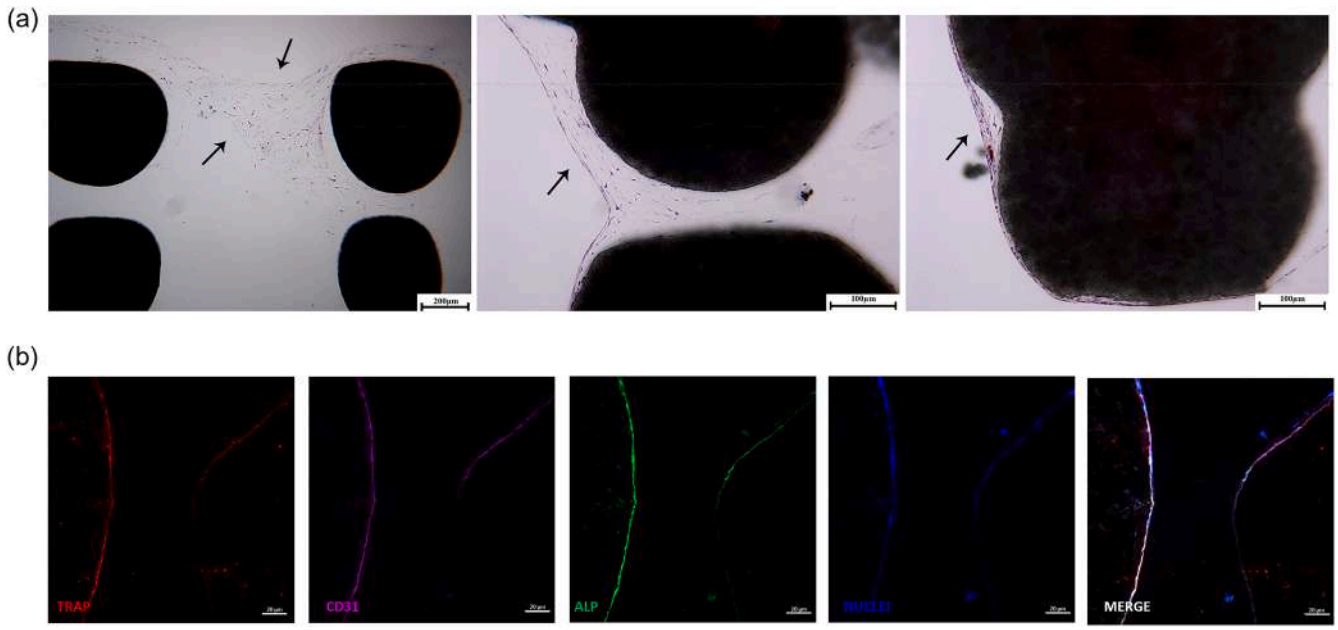

Fig. 8. hOBs/hMCs/HUVECs cultured on the BCP scaffold. a Acid fuchsine and toluidine blue staining evaluated through histological analysis; **b** the expression of TRAP (red staining), CD31 (purple staining), and ALP (green staining), markers of osteoclasts, HUVECs, and hOBs, respectively, evaluated by IF analyses. Cells nuclei were stained in blue with DAPI.

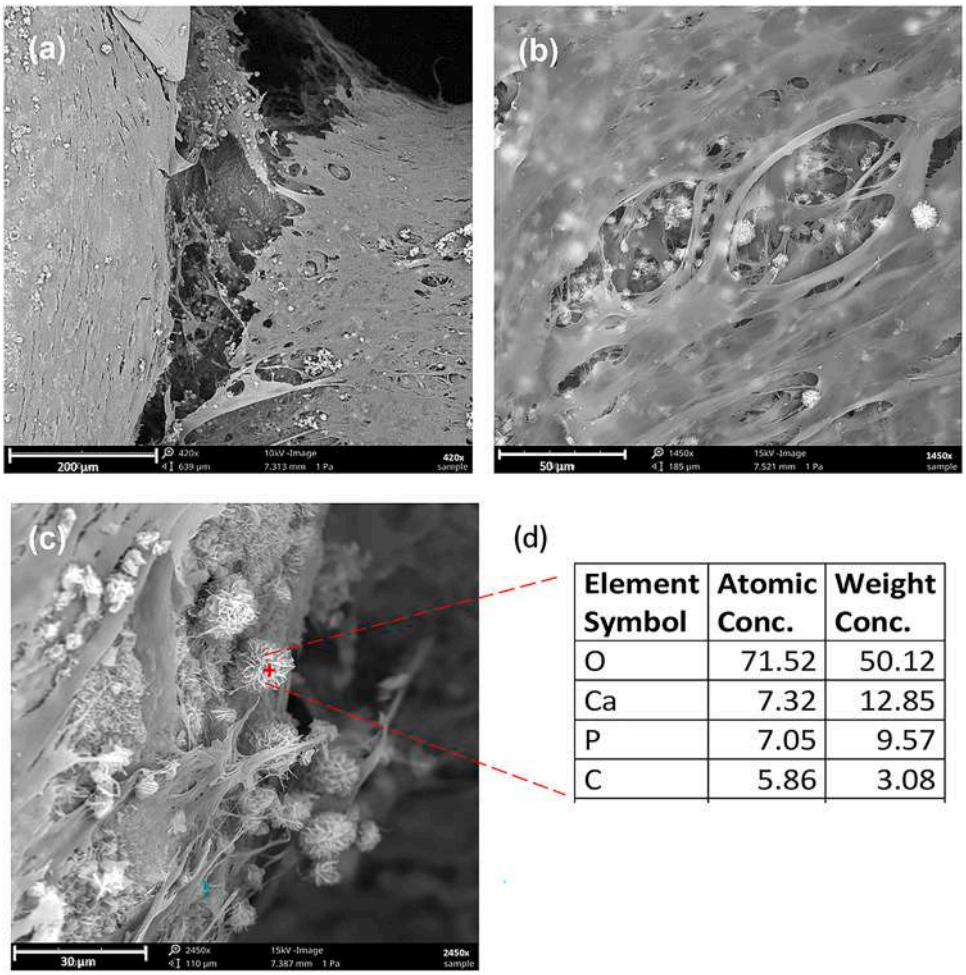

Element Symbol	Atomic Conc.	Weight Conc.
O	71.52	50.12
Ca	7.32	12.85
P	7.05	9.57
C	5.86	3.08

Fig. 9. SEM analyses the tri-culture system. a-c SEM images at different magnifications representing hOBs/hMCs/HUVECs cultured on the BCP scaffold after 14 days in OM. SEM images and **d** the energy-dispersive X-ray spectroscopy (EDX) analyses showed mineralized crystals released from cells.

demonstrating the osteoconductive capabilities of the scaffold. Additionally, SEM and EDX analyses conducted on the tri-culture system indicated the deposition of mineralized matrix crystals within this tissue-like cellular layer, further suggesting the potential osteoinductive properties of the BCP scaffold. Based on these findings, we hypothesize that the combined osteoconductive and osteoinductive properties of our BCP scaffold facilitated cellular interactions. This led to the formation of a bone-like cell layer characterized by mineralized matrix crystals while preserving the native phenotypes of hOBs, hMCs, and HUVECs. Indeed, as demonstrated by IF results, all three cell types maintained the expression of their specific osteoblastic, osteoclastic, and endothelial markers, such as ALP, TRAP, and CD31, after 14 days of co-culture. Notably, all experiments in our tri-culture cellular model were carried out without the addition of exogenous stimuli such as VEGF, MCSF, RANKL, or BMPs, thus taking advantage of the cellular physiological ability to drive individual phenotypes. In this scenario, the choice of hOBs derived from vertebral lamina was intentional, given their already known greater osteogenic capabilities [54].

Regarding the localization of cells seeded on the BCP scaffold, our IF results corroborate recent findings by Lu T. and collaborators [55], showing that hOBs and hMCs predominantly localized and exhibited significant growth on the BCP scaffold outskirts. This observation is further supported by the outcomes of co-culture experiments exclusively involving bone cells seeded on the BCP scaffold. Contrarily, when examining the behavior of vascular cells, both in monoculture and tri-culture experiments, we observed a predominant migration of HUVECs toward the scaffold core, displaying an elongated morphology (spindle shape) and forming tube-like structures. These findings align with a recent study [56], which suggests that viable CD31-expressing HUVECs may activate the angiogenic process after 14 days of co-culture.

The *in vitro* results obtained from SEM and IF were also corroborated by histological indications, indicating that the BCP scaffold can be considered a suitable substrate for the growth and proliferation of osteoblasts, osteoclasts, and endothelial cells. Indeed, the presence of cell cordons and a dense cell layer within the pores (>300 μm) of the scaffold suggests that cell invasion occurred in the internal portion, as observed in other studies [57,58]. In addition, the colonization of the BCP scaffold surface has also been demonstrated in prior research [59,60].

However, a limitation of this study is that it relies solely on observational data, as quantitative assessments of cellular activity related to bone neoformation and neovascularization were not provided. The activation of these processes is inferred only from the observation of mineralized matrix crystals and tubular-like formations. This is primarily because the main objective of the study was to evaluate the BCP scaffold from morphometric and biomechanical perspectives and subsequently assess its effects on cell behavior. Nevertheless, unlike previous studies that employed mono- or dual-cell cultures, this research successfully demonstrated not only the optimal morphometry and biomechanics of the BCP scaffold but also the effective co-cultivation of three distinct cell types on the BCP scaffold, highlighting the biological properties of this latter [41,55,59,60].

5. Conclusions

In conclusion, the high performance of the BCP scaffold, validated with biomechanical studies and the preservation of osteoblast, osteoclast, and endothelial cell phenotypes *in vitro*, highlights its potential for developing a 3D *in vitro* model that mimics the oral microenvironment. This model could be valuable for the regeneration of critical jawbone defects in BTE approaches. Therefore, researchers can more effectively translate their findings to *in vivo* models and, ultimately, to clinical applications aimed at promoting jawbone regeneration and treating bone-related disorders. Furthermore, it is crucial to emphasize that further studies could expand the potential applications of this scaffold model beyond bone regeneration in the oral field to other orthopedics sites.

CRediT authorship contribution statement

Domitilla Mandatori: Writing – review & editing, Writing – original draft, Methodology, Conceptualization. **Emira D'Amico:** Writing – review & editing, Writing – original draft, Methodology. **Tea Romasco:** Writing – review & editing, Investigation. **Maria Laura Gatto:** Writing – review & editing, Investigation. **Maria Pina Notarangelo:** Writing – review & editing, Investigation. **Carlo Mangano:** Writing – review & editing, Methodology. **Michele Furlani:** Writing – review & editing, Methodology. **Letizia Penolazzi:** Writing – review & editing, Writing – original draft, Methodology, Conceptualization.

Declaration of competing interest

The authors declare that they have no known competing financial interests or personal relationships that could have appeared to influence the work reported in this paper.

Data availability

The datasets used and analyzed in this study are available from the corresponding author upon reasonable request.

Ethical approval

Human osteoblasts (hOBs) were obtained from vertebral lamina samples discarded during spinal surgery following research protocol approved by the Ethics Committee of the S. Anna Hospital (protocol no 160998). Human monocytes (hMCs) were isolated from peripheral blood of healthy donors after informed consent (protocol no 0110952). Human umbilical vein endothelial cells (HUVECs) were isolated from umbilical cords collectedfrom randomly selected healthy Caucasian mothers at the Hospital of Chieti and Pescara (Italy) (protocol no.1879/09COET). All procedures adhered to the ethical standards of the Institutional Committee on Human Experimentation and with the Declaration of Helsinki Principles. The patients/participants provided their written informed consent to biological samples collection.

Acknowledgments

This publication has emanated from research conducted with the financial support of: PON-MISE Sustainable Growth Funding-DD27 September 2018 (grant no 21, F/180021/03/X43).

Fondo di Ateneoper la Ricerca Scientifica (FAR 2023 grants to Letizia Penolazzi).

Domitilla Mandatori is a researcher (code n. 53-I-14751–1) supported by PON R&I "Ricerca e Innovazione" 2014–2020, Action IV.4 "Doctorates and research contracts on innovation issues", DM 1061/2021, funded by the Ministry of University and Research (MUR), Italy, FSE REACT-EU.

Finally, we also thank Dr Daniel Seitz (Biomed Center Innovation gGmbH, Bayreuth, Germany) for biomaterial providing; Dr Nicole Riberti, Dr Tania Vanessa Pierfelice and Dr Elisabetta Lambertini for their technical support; Dr Natalia Di Pietro, Prof. Assunta Pandolfi, Prof. Roberta Piva, Prof. Giovanna Iezzi and Prof. Alessandra Giuliani for their supervision.

Supplementary materials

Supplementary material associated with this article can be found, in the online version, at doi:10.1016/j.jdent.2024.105411.

References

[1] J.F. Keating, A.H. Simpson, C.M. Robinson, The management of fractures with bone loss, J. Bone. Joint Surg. Br. 87 (2) (2005) 142–150, https://doi.org/10.1302/0301-620x.87b2.15874.

[2] A. Sakkas, F. Wilde, M. Heufelder, et al., Autogenous bone grafts in oral implantology-is it still a "gold standard"? A consecutive review of 279 patients with 456 clinical procedures, Int. J. Implant. Dent. 3 (1) (2017) 23, https://doi.org/10.1186/s40729-017-0084-4.

[3] T.J. Blokhuis, J.J. Arts, Bioactive and osteoinductive bone graft substitutes: definitions, facts and myths, Injury 42 (Suppl 2) (2011) S26–S29, https://doi.org/10.1016/j.injury.2011.06.010.

[4] F.E. Freeman, D.C. Browe, J. Nulty, et al., Biofabrication of multiscale bone extracellular matrix scaffolds for bone tissue engineering, Eur. Cell Mater. 38 (2019) 168–187, https://doi.org/10.22203/eCM.v038a12.

[5] C. Mangano, F. Mangano, L. Gobbi, et al., Comparative Study between Laser Light Stereo-Lithography 3D-Printed and Traditionally Sintered Biphasic Calcium Phosphate Scaffolds by an Integrated Morphological, Morphometric and Mechanical Analysis, Int. J. Mol. Sci. 20 (13) (2019), https://doi.org/10.3390/ijms20133118.

[6] C. Mangano, A. Giuliani, I. De Tullio, et al., Case Report: histological and Histomorphometrical Results of a 3-D Printed Biphasic Calcium Phosphate Ceramic 7 Years After Insertion in a Human Maxillary Alveolar Ridge, Front. Bioeng. Biotechnol. 9 (2021) 614325, https://doi.org/10.3389/fbioe.2021.614325.

[7] A. Giuliani, S. Mazzoni, L. Mele, et al., Synchrotron Phase Tomography: an Emerging Imaging Method for Microvessel Detection in Engineered Bone of Craniofacial Districts, Front Physiol 8 (2017) 769, https://doi.org/10.3389/fphys.2017.00769.

[8] V. Mastrullo, W. Cathery, E. Velliou, et al., Angiogenesis in Tissue Engineering: as Nature Intended? Front. Bioeng. Biotechnol. 8 (2020) 188, https://doi.org/10.3389/fbioe.2020.00188.

[9] J. Rouwkema, A. Khademhosseini, Vascularization and Angiogenesis in Tissue Engineering: beyond Creating Static Networks, Trends Biotechnol. 34 (9) (2016) 733–745, https://doi.org/10.1016/j.tibtech.2016.03.002.

[10] H. Liu, H. Chen, Q. Han, et al., Recent advancement in vascularized tissue-engineered bone based on materials design and modification, Mater Today Bio 23 (2023) 100858, https://doi.org/10.1016/j.mtbio.2023.100858.

[11] A. Giuliani, A. Manescu, S. Mohammadi, et al., Quantitative Kinetics Evaluation of Blocks Versus Granules of Biphasic Calcium Phosphate Scaffolds (HA/beta-TCP 30/70) by Synchrotron Radiation X-ray Microtomography: a Human Study, Implant Dent. 25 (1) (2016) 6–15, https://doi.org/10.1097/ID.0000000000000363.

[12] E. Tsuruga, H. Takita, H. Itoh, et al., Pore size of porous hydroxyapatite as the cell-substratum controls BMP-induced osteogenesis, J. Biochem. 121 (2) (1997) 317–324, https://doi.org/10.1093/oxfordjournals.jbchem.a021589.

[13] Y. Kuboki, Q. Jin, H. Takita, Geometry of carriers controlling phenotypic expression in BMP-induced osteogenesis and chondrogenesis, J. Bone. Joint Surg. Am. 83-A (Suppl 1 (Pt 2)) (2001) S105–S115.

[14] M.N. Hassan, M.A. Yassin, S. Suliman, et al., The bone regeneration capacity of 3D-printed templates in calvarial defect models: a systematic review and meta-analysis, Acta Biomater. 91 (2019) 1–23, https://doi.org/10.1016/j.actbio.2019.04.017.

[15] C. Mangano, B. Sinjari, J.A. Shibli, et al., A Human Clinical, Histological, Histomorphometrical, and Radiographical Study on Biphasic HA-Beta-TCP 30/70 in Maxillary Sinus Augmentation, Clin. Implant Dent. Relat. Res. 17 (3) (2015) 610–618, https://doi.org/10.1111/cid.12145.

[16] A. Giuliani, A. Manescu, M. Langer, et al., Three years after transplants in human mandibles, histological and in-line holotomography revealed that stem cells regenerated a compact rather than a spongy bone: biological and clinical implications, Stem Cells Transl Med 2 (4) (2013) 316–324, https://doi.org/10.5966/sctm.2012-0136.

[17] F. Paino, M. La Noce, A. Giuliani, et al., Human DPSCs fabricate vascularized woven bone tissue: a new tool in bone tissue engineering, Clin. Sci. (Lond.) 131 (8) (2017) 699–713, https://doi.org/10.1042/CS20170047.

[18] D.W. Sanders, M. Bhandari, G. Guyatt, et al., Critical-sized defect in the tibia: is it critical? Results from the SPRINT trial, J. Orthop. Trauma 28 (11) (2014) 632–635, https://doi.org/10.1097/BOT.0000000000000194.

[19] M.H. Syahruddin, R. Anggraeni, I.D. Ana, A microfluidic organ-on-a-chip: into the next decade of bone tissue engineering applied in dentistry, Future Sci OA 9 (10) (2023) FSO902, https://doi.org/10.2144/fsoa-2023-0061.

[20] C. Lei, J. Lei, X. Zhang, et al., Heterostructured piezocatalytic nanoparticles with enhanced ultrasound response for efficient repair of infectious bone defects, Acta Biomater. 172 (2023) 343–354, https://doi.org/10.1016/j.actbio.2023.10.006.

[21] M. Laubach, F. Hildebrand, S. Suresh, et al., The concept of scaffold-guided bone regeneration for the treatment of long bone defects: current clinical application and future perspective, J Funct Biomater 14 (7) (2023), https://doi.org/10.3390/jfb14070341.

[22] R. Bagherpour, G. Bagherpour, P. Mohammadi, Application of artificial intelligence in tissue engineering, Tissue Eng Part B Rev (2024), https://doi.org/10.1089/ten.TEB.2024.0022.

[23] B. Zhao, Q. Peng, R. Zhou, et al., Precision medicine in tissue engineering on bone, Methods Mol. Biol. 2204 (2020) 207–215, https://doi.org/10.1007/978-1-0716-0904-0_18.

[24] J.P.K. Armstrong, M.M. Stevens, Emerging technologies for tissue engineering: from gene editing to personalized medicine, Tissue Eng. Part A 25 (9–10) (2019) 688–692, https://doi.org/10.1089/ten.TEA.2019.0026.

[25] D. Zhao, Q. Saiding, Y. Li, et al., Bone organoids: recent advances and future challenges, Adv. Healthc. Mater. 13 (5) (2024) e2302088, https://doi.org/10.1002/adhm.202302088.

[26] X. Yang, J. Jiang, L. Zhou, et al., Osteogenic and angiogenic characterization of mandible and femur osteoblasts, J. Mol. Histol. 50 (2) (2019) 105–117, https://doi.org/10.1007/s10735-019-09810-6.

[27] F. Fazan, K.B. Shahida, Fabrication of synthetic apatites by solid-state reactions, Med. J. Malaysia 59 (Suppl B) (2004) 69–70.

[28] G. Daculsi, R.Z. LeGeros, E. Nery, et al., Transformation of biphasic calcium phosphate ceramics in vivo: ultrastructural and physicochemical characterization, J. Biomed. Mater. Res. 23 (8) (1989) 883–894, https://doi.org/10.1002/jbm.820230806.

[29] G.-C.J.M. Vallet-Regí Marí, Calcium phosphates as substitution of bone tissues, Prog. Solid State Chem. 32 (1–2) (2004) 1–31, https://doi.org/10.1016/j.progsolidstchem.2004.07.001.

[30] X. Xiao, W. Wang, D. Liu, et al., The promotion of angiogenesis induced by three-dimensional porous beta-tricalcium phosphate scaffold with different interconnection sizes via activation of PI3K/Akt pathways, Sci. Rep. 5 (2015) 9409, https://doi.org/10.1038/srep09409.

[31] U. Deisinger, Generating porous ceramic scaffolds: processing and properties, Key Eng. Mater. 441 (2010) 155–179.

[32] E. Lambertini, L. Penolazzi, G. Pellielo, et al., Pro-Osteogenic properties of violina pumpkin (cucurbita moschata) leaf extracts: data from in vitro human primary cell cultures, Nutrients 13 (8) (2021), https://doi.org/10.3390/nu13082633.

[33] L. Penolazzi, E. Tavanti, R. Vecchiatini, et al., Encapsulation of mesenchymal stem cells from Wharton's jelly in alginate microbeads, Tissue Eng Part C Methods 16 (1) (2010) 141–155, https://doi.org/10.1089/ten.TEC.2008.0582.

[34] W. Wang, K.W.K. Yeung, Bone grafts and biomaterials substitutes for bone defect repair: a review, Bioact Mater 2 (4) (2017) 224–247, https://doi.org/10.1016/j.bioactmat.2017.05.007.

[35] C.M. Misch, Use of the mandibular ramus as a donor site for onlay bone grafting, J. Oral Implantol. 26 (1) (2000) 42–49, https://doi.org/10.1563/1548-1336(2000)026<0042:UOTMRA>2.3.CO;2.

[36] D. Buser, I. Urban, A. Monje, et al., Guided bone regeneration in implant dentistry: basic principle, progress over 35 years, and recent research activities, Periodontol 2000 93 (1) (2023) 9–25, https://doi.org/10.1111/prd.12539.

[37] C. Mangano, G. Luongo, F. Luongo, et al., Custom-made computer-aided-design/computer-assisted-manufacturing (CAD/CAM) synthetic bone grafts for alveolar ridge augmentation: a retrospective clinical study with 3 years of follow-up, J. Dent. 127 (2022) 104323, https://doi.org/10.1016/j.jdent.2022.104323.

[38] R. Zhao, R. Yang, P.R. Cooper, et al., Bone grafts and substitutes in dentistry: a review of current trends and developments, Molecules 26 (10) (2021), https://doi.org/10.3390/molecules26103007.

[39] D. Shopova, A. Mihaylova, A. Yaneva, et al., Advancing dentistry through bioprinting: personalization of oral tissues, J Funct Biomater 14 (10) (2023), https://doi.org/10.3390/jfb14100530.

[40] J. Giron, E. Kerstner, T. Medeiros, et al., Biomaterials for bone regeneration: an orthopedic and dentistry overview, Braz. J. Med. Biol. Res. 54 (9) (2021) e11055, https://doi.org/10.1590/1414-431x2021e11055.

[41] J. Feng, J. Liu, Y. Wang, et al., Beta-TCP scaffolds with rationally designed macro-micro hierarchical structure improved angio/osteo-genesis capability for bone regeneration, J. Mater. Sci. Mater. Med. 34 (7) (2023) 36, https://doi.org/10.1007/s10856-023-06733-3.

[42] V.A. Reyna-Urrutia, M. Estevez, A.M. Gonzalez-Gonzalez, et al., 3D scaffolds of caprolactone/chitosan/polyvinyl alcohol/hydroxyapatite stabilized by physical bonds seeded with swine dental pulp stem cell for bone tissue engineering, J. Mater. Sci. Mater. Med. 33 (12) (2022) 81, https://doi.org/10.1007/s10856-022-06702-2.

[43] P.P. Jung-Hwan Lee, Jin Guang-Zhen, J.C. Knowles, Hae-Won Kim Materials roles for promoting angiogenesis in tissue regeneration, Prog. Mater Sci. 117 (2021) 100732, https://doi.org/10.1016/j.pmatsci.2020.100732. Get rights and content.

[44] V. Wu, M.N. Helder, N. Bravenboer, et al., Bone tissue regeneration in the oral and maxillofacial region: a review on the application of stem cells and new strategies to improve vascularization, Stem Cells Int 2019 (2019) 6279721, https://doi.org/10.1155/2019/6279721.

[45] A. Giuliani, M.L. Gatto, L. Gobbi, et al., Integrated 3D information for custom-made bone grafts: focus on biphasic calcium phosphate bone substitute biomaterials, Int. J. Environ. Res. Public Health 17 (14) (2020), https://doi.org/10.3390/ijerph17144931.

[46] S. Zhu, S. Ehnert, M. Rouss, et al., From the clinical problem to the basic research-co-culture models of osteoblasts and osteoclasts, Int. J. Mol. Sci. 19 (8) (2018), https://doi.org/10.3390/ijms19082284.

[47] M.A. Velasco, C.A. Narvaez-Tovar, D.A. Garzon-Alvarado, Design, materials, and mechanobiology of biodegradable scaffolds for bone tissue engineering, Biomed. Res. Int. 2015 (2015) 729076, https://doi.org/10.1155/2015/729076.

[48] G.L. Koons, M. Diba, A.G. Mikos, Materials design for bone-tissue engineering, Nat. Rev. Mater. 5 (2020) 584–603, https://doi.org/10.1038/s41578-020-0204-2.

[49] G. Iezzi, A. Scarano, L. Valbonetti, et al., Biphasic calcium phosphate biomaterials: stem cell-derived osteoinduction or in vivo osteoconduction? Novel insights in maxillary sinus augmentation by advanced imaging, Materials (Basel) 14 (9) (2021), https://doi.org/10.3390/ma14092159.

[50] A. Grosso, M.G. Burger, A. Lunger, et al., It Takes Two to Tango: coupling of Angiogenesis and Osteogenesis for Bone Regeneration, Front. Bioeng. Biotechnol. 5 (2017) 68, https://doi.org/10.3389/fbioe.2017.00068.

[51] E. Ellermann, N. Meyer, R.E. Cameron, et al., *In vitro* angiogenesis in response to biomaterial properties for bone tissue engineering: a review of the state of the art, Regen Biomater 10 (2023) rbad027, https://doi.org/10.1093/rb/rbad027.
[52] C. Li, G. Chen, Y. Wang, et al., Indirect co-culture of osteoblasts and endothelial cells *in vitro* based on a biomimetic 3D composite hydrogel scaffold to promote the proliferation and differentiation of osteoblasts, PLoS One 19 (3) (2024) e0298689, https://doi.org/10.1371/journal.pone.0298689.
[53] M. Bi, K. Yang, T. Yu, et al., Cell-based mechanisms and strategies of co-culture system both *in vivo* and vitro for bone tissue engineering, Biomed. Pharmacother. 169 (2023) 115907, https://doi.org/10.1016/j.biopha.2023.115907.
[54] E. Lambertini, L. Penolazzi, M. Angelozzi, et al., The expression of cystathionine gamma-lyase is regulated by estrogen receptor alpha in human osteoblasts, Oncotarget 8 (60) (2017) 101686–101696, https://doi.org/10.18632/oncotarget.21514.
[55] T.Y.X Lu, L. Zhang, F. He, X. Wang, J. Ye, Enhancing osteoinduction and bone regeneration of biphasic calcium phosphate scaffold thought modulating the balance between pro-osteogenesis and anti-osteoclastogenesis by zinc doping, Mater. Today Chem. 29 (2023) 101410, https://doi.org/10.1016/j.mtchem.2023.101410.
[56] E. Alfayez, L. Veschini, M. Dettin, et al., DAR 16-II Primes Endothelial Cells for Angiogenesis Improving Bone Ingrowth in 3D-Printed BCP Scaffolds and Regeneration of Critically Sized Bone Defects, Biomolecules 12 (11) (2022), https://doi.org/10.3390/biom12111619.
[57] C.M. Murphy, F.J. O'Brien, Understanding the effect of mean pore size on cell activity in collagen-glycosaminoglycan scaffolds, Cell Adh. Migr. 4 (3) (2010) 377–381, https://doi.org/10.4161/cam.4.3.11747.
[58] Y. Han, M. Lian, Q. Wu, et al., Effect of pore size on cell behavior using melt electrowritten scaffolds, Front. Bioeng. Biotechnol. 9 (2021) 629270, https://doi.org/10.3389/fbioe.2021.629270.
[59] S.N. Rath, L.A. Strobel, A. Arkudas, et al., Osteoinduction and survival of osteoblasts and bone-marrow stromal cells in 3D biphasic calcium phosphate scaffolds under static and dynamic culture conditions, J. Cell. Mol. Med. 16 (10) (2012) 2350–2361, https://doi.org/10.1111/j.1582-4934.2012.01545.x.
[60] P. Pereira, A.S. Neto, A.S. Rodrigues, et al., In vitro evaluation of biphasic calcium phosphate scaffolds derived from cuttlefish bone coated with Poly(ester urea) for bone tissue regeneration, Polymers (Basel) 15 (10) (2023), https://doi.org/10.3390/polym15102256.